HHS Public Access

Author manuscript

Magn Reson Med. Author manuscript; available in PMC 2018 April 01.

Published in final edited form as:

Magn Reson Med. 2017 April ; 77(4): 1446–1458. doi:10.1002/mrm.26216.

MR Fingerprinting for Rapid Quantification of Myocardial T_1, T_2, and Proton Spin Density

Jesse I. Hamilton[1], **Yun Jiang**[1], **Yong Chen**[2], **Dan Ma**[1], **Wei-Ching Lo**[1], **Mark Griswold**[1,2], and **Nicole Seiberlich**[1,2]

[1]Biomedical Engineering, Case Western Reserve University, USA

[2]Radiology, University Hospitals Case Medical Center, USA

Abstract

Purpose—To introduce a 2D MR Fingerprinting technique for quantification of T_1, T_2, and M_0 in myocardium.

Methods—An ECG-triggered MR Fingerprinting (MRF) method is introduced for mapping myocardial T_1, T_2, and M_0 during a single breathhold in as short as four heartbeats. The pulse sequence employs variable flip angles, repetition times, inversion recovery times, and T_2 preparation dephasing times. A dictionary of possible signal evolutions is simulated for each scan that incorporates the subject's unique variations in heart rate. Aspects of the sequence design were explored in simulations, and the accuracy and precision of cardiac MRF were assessed in a phantom study. In vivo imaging was performed at 3T in eleven volunteers to generate native parametric maps.

Results—T_1 and T_2 measurements from the proposed cardiac MRF sequence correlated well with standard spin echo measurements in the phantom study (R^2>0.99). A Bland-Altman analysis revealed good agreement for myocardial T_1 measurements between MRF and MOLLI (bias 1ms, 95% limits of agreement −72 to 72ms) and T_2 measurements between MRF and T_2-prepared bSSFP (bias −2.6ms, 95% limits of agreement −8.5 to 3.3ms).

Conclusions—MRF can provide quantitative single slice T_1, T_2, and M_0 maps in the heart within a single breathhold.

Introduction

Quantitative parameter mapping in the myocardium has gained attention due to its potential to identify pathological changes earlier than traditional qualitative imaging (1,2). Whereas the image contrast in qualitative scans is weighted by proton spin density and the T_1 and T_2 relaxation times, parameter mapping enables pixelwise measurements of these intrinsic tissue properties. Changes in native T_1 measurements have been associated with inflammation (3), acute (4) and possibly chronic (5,6) myocardial scar, and restructuring of the extracellular matrix caused by fibrosis (7,8). In addition, T_1 maps collected before and after injection of contrast medium can be used to calculate the extracellular volume fraction,

Correspondence to: Jesse I. Hamilton.

which can identify diffuse fibrosis that is difficult to detect on late gadolinium enhancement scans (9–11). Native T_2 maps provide diagnostic information regarding edema (12,13), heart transplant rejection (14), and acute inflammatory disease and myocarditis (15).

Several MRI pulse sequences have been developed for mapping T_1, T_2, or both simultaneously in the myocardium. T_1 mapping can be performed with a modified inversion recovery technique, such as MOLLI and its derivatives (16,17), or with saturation recovery methods like SASHA (18). These techniques typically work by acquiring several images with different effective TI times using a single-shot or segmented readout. At each pixel, the measured signals are fit to a two- or three-parameter exponential signal equation to estimate T_1. Similarly, T_2 can be measured with fast spin echo (19,20), GRASE (21), or balanced SSFP pulse sequences that are preceded by T_2 preparation pulses with different dephasing times (13,22). Some sequences have also been proposed for performing simultaneous T_1 and T_2 measurements in the myocardium within a single breathhold (23–26).

However, most cardiac quantitative mapping sequences still resemble a conventional inversion recovery or spin echo experiment, with a common theme of preparing the magnetization and then sampling different portions along an exponential recovery or decay curve. A sufficient number of data points must be sampled in order to accurately characterize the curve. The parameter estimation method (e.g. two-parameter vs three-parameter) can also influence the accuracy and precision of the maps (27). Physiological motion can be a major hurdle, with many sequences employing a breathhold and using ECG triggering to minimize motion artifacts. In particular, variations in heart rate can lead to bias in the parameter maps, as has been reported with MOLLI at fast heart rates (17).

MR Fingerprinting (MRF) has recently been introduced for quantifying multiple parameters within a single scan (28,29) and is a promising new approach for rapid relaxation time mapping. MRF intentionally avoids steady state imaging and instead uses a pseudorandom pulse sequence, which causes different tissues to produce unique signal evolutions over time due to their characteristic MR parameters, such as T_1 and T_2. The measured signal timecourses for each pixel are matched to a dictionary of simulated signal evolutions in order to create quantitative maps. MRF is able to achieve high scan efficiency and robustness to noise and motion due to the use of the pattern matching approach, which is less sensitive to factors that can corrupt the acquired data.

This study aims to modify MRF for parametric mapping of T_1, T_2, and M_0 in the myocardium, where physiological motion must be taken into consideration. The scan uses ECG triggering with a diastolic readout and can be performed during a single breathhold in as short as four heartbeats. Whereas the original MRF sequence has a prescribed sequence timing such that the dictionary can be precalculated, the timing of cardiac MRF depends on the subject's heart rate, so a new dictionary is calculated for every scan. The creation of scan-specific dictionaries makes cardiac MRF robust to differences in heart rates, as demonstrated in simulations. Additionally, phantom studies are presented to validate T_1 and T_2 measurements from cardiac MRF against conventional spin echo measurements, and MRF is compared with MOLLI and a T_2-prepared bSSFP mapping sequence in eleven healthy volunteers at 3T.

Methods

Pulse Sequence

The cardiac MRF pulse sequence (Figure 1A) was designed with the goal of encoding different tissue types, which have distinct combinations of T_1 and T_2, with unique temporal signal evolutions or "fingerprints". Data are acquired during a breathhold lasting up to sixteen heartbeats (although shorter scan times are possible, as discussed later), and ECG triggering restricts the RF excitation and data readout to end diastole in order to reduce artifacts from cardiac motion. Every heartbeat begins with a constant trigger delay and is followed by a 240–280ms acquisition window, which varies slightly in duration among heartbeats due to the variable TRs. Highly undersampled (R=48) images are acquired using a single interleaf of a variable density spiral trajectory, with 48 images collected every heartbeat to yield 48x16=768 images over the entire scan. Because of the challenges posed by off-resonance artifacts at 3T, a FISP readout is used with refocused x- and y-gradients and a spoiler on the slice select axis at the end of every TR that produces a phase twist of 8π across the voxel (29).

In the spirit of previous MRF work, the flip angles and TRs vary throughout the scan, and magnetization preparation pulses are used to further enhance the sensitivity to T_1 and T_2. Sinusoidally varying flip angles were generated according to $FA(n)=A\cdot\sin\left(\frac{2\pi n}{3T}\right)+B$, where B=4°, T=48 is the number of excitations per heartbeat, A is a number between 0–11° selected using a random number generator that changes for each heartbeat, and $1\leq n\leq T$ is the index of the RF excitation within the current heartbeat. The flip angles are constrained to be small (less than 15°) in order to minimize the effects of inhomogenous B_1^+ and imperfect slice profiles (see Discussion). The TR pattern was created using a Perlin noise distribution (30) and varies between 5.1–6.1ms, with the smallest TR dictated by scanner hardware limits and the spiral k-space trajectory. To improve the sensitivity to T_1, a non-selective adiabatic inversion pulse is played at a time TI before the scan window every four heartbeats. The TI is varied between 21–400ms. If the maximum TI of 400ms does not fit within one cardiac cycle because of a rapid heart rhythm, then it is set to be equal to the trigger delay. In addition, an MLEV composite T_2-preparation pulse (31) with dephasing time TE of either 40 or 80ms is played immediately before the scan window for half of the heartbeats.

As described in (28), a k-space trajectory is chosen that produces spatially and temporally incoherent artifacts when undersampled, which aids in the pattern matching step. Data are sampled along a variable density spiral having a minimum time gradient design (32), which requires 24 interleaves to fully sample the center 25% of k-space and 48 interleaves to completely satisfy the Nyquist criterion at the edges of a 192x192 k-space matrix. A time series of undersampled (acceleration factor R=48) images is generated by gridding each single-shot interleaf using the NUFFT (33). Individually, each image is degraded by severe aliasing artifacts. The spiral arm is rotated by the golden angle (111°) after each excitation, which shifts the position of the artifacts over time.

Dictionary Generation

At each pixel, the signal intensity timecourse from the undersampled images is matched to the MRF dictionary to extract quantitative information. The dictionary is a lookup table that links discrete pairs of T_1 and T_2 with a characteristic signal evolution. A Bloch simulation is performed using an isochromat of 250 spins, and the MRF signal is calculated by taking the complex average of the transverse magnetization over the entire isochromat at the echo time. Some residual transverse magnetization remains after each TR due to the gradient spoiling, which was modeled by simulating a phase twist of 8π along one axis. The dictionary resolution, denoted by min:step:max, was $T_1 \in$ [50:10:2000, 2020:20:3000, 3050:50:5000 ms] and $T_2 \in$ [6:2:100 105:5:200, 220:20:500] ms, and the dictionary had a total of 14,166 entries. Unrealistic pairs of T_1 and T_2 were not simulated, including $T_2 > T_1$.

Because the subject's heart rate can change throughout the scan, a variable amount of time elapses between the end of one acquisition window and the first excitation in the next acquisition window. These times are accounted for in the Bloch simulation by recording the timestamp associated with each RF excitation. A new dictionary is generated after every scan that incorporates these variable timings. This is different from other MRF approaches that use a predetermined pulse sequence, where the dictionary only needs to be computed once and can be applied to all subsequent scans. The individualized cardiac MRF dictionaries were generated using MATLAB Mex code and took an average of 12.1s to compute on a desktop PC (Dell XPS 8500, 3.40 GHz, Intel i7 Core, 16 GB RAM).

Pattern Recognition

Quantitative maps were generated by matching the measured MRF signal timecourses to the dictionary using an iterative multiscale pattern recognition (shown schematically in Figure 2) (34). This algorithm requires knowledge of the coil sensitivity maps, and these were estimated using the Walsh method (35) with images generated by combining all of the spiral interleaves over time. In each iteration of the pattern recognition scheme, the k-space data were lowpass filtered with a 2D Gaussian function, gridded, and converted to the image domain. The uncombined coil images were multiplied by the complex conjugate of the coil maps and summed over the coil dimension. The combined coil images had reduced spatial resolution but also fewer aliasing artifacts. Pattern matching was performed by taking the complex-valued dot product between each pixel's signal timecourse with the dictionary and finding the entry with the largest correlation. Proton density was calculated as the scaling factor needed to match the amplitude of the measured signal with the dictionary entry. A small total variation penalty was applied to the intermediate T_1 and T_2 maps at this stage. New MRF signal evolutions were simulated from the intermediate maps and multiplied by the coil sensitivity profiles to yield multi-channel data. After converting the data back into k-space, data consistency was enforced by replacing the acquired k-space data at the sampled locations. This process was repeated with less aggressive Gaussian filtering until the maximum number of iterations was reached. In this work, six iterations were used with Gaussian filter widths of 10%, 18%, 32%, 56% and 100% of k_{max}, and no filtering on the sixth iteration. The computation time for a 192x192 slice with 768 undersampled images was 7min, 50s for the iterative reconstruction compared to 33s for direct pattern matching.

Figure 3 shows T_1 and T_2 maps after different iterations, as well as the raw signal evolutions for one pixel in the myocardium and the closest match in the dictionary.

Simulations

Several simulations were performed to explore properties of the MRF reconstruction. An open-source numerical cardiac phantom (MRXCAT) was modified to have T_1 and T_2 values previously reported at 3T (36). The phantom contained T_1 values from 370 to 1930ms and T_2 from 20 to 275ms, with a myocardial T_1 of 1410ms and T_2 of 50ms. Because data are acquired during a breathhold with ECG triggering, no motion was incorporated in the simulation. The first simulation was intended to guide the MRF pulse sequence design. A four-heartbeat scan was simulated assuming a constant heart rate of 60bpm. The following design parameters were studied: (1) the use of variable rather than constant flip angles and Rs, (2) the maximum flip angle, and (3) the presence or absence of magnetization preparation pulses. For these simulations, the maximum flip angle was varied between 15° to 75° in steps of 10°. The variable FA/TR pattern (Figure 1A) was designed empirically to start from a small flip angle (4°) every heartbeat and increase gradually to larger values. This property reduced high frequency oscillations in the MRF signal evolutions and was expected to improve the pattern recognition (see Discussion). When testing different sequences, this pattern was scaled to attain the desired maximum flip angle. The constant FA/TR pattern used the minimum TR of 5.1ms to maximize the amount of data collected and a flip angle equal to the desired maximum value. In all, twenty-eight different MRF sequences were tested (Table 1). MRF signal evolutions were generated for the phantom using simulated coil sensitivity profiles with eight channels, and the k-space data were undersampled as described earlier. The iterative pattern matching was performed, and accuracy was quantified over the entire phantom using the normalized $\mathrm{RMSE}\left|\frac{estimated-truth}{truth}\right| \times 100\%$.

The second simulation was performed using the two sequences having the lowest T_1 and T_2 RMSE from the previous simulation. Specifically, these sequences used variable and constant FA/TR patterns having a maximum flip angle of 15° with magnetization preparation pulses. The reconstructions were repeated for different scan durations from two to sixteen heartbeats. In addition, the pattern recognition was implemented using both direct matching (i.e. complex dot product, as in the original implementation of MRF) and the iterative multiscale matching. A third simulation evaluated the effect of a time-varying heart rate on the quantification accuracy. The four-heartbeat MRF sequence with variable FA/TR was simulated using an artificial cardiac cycle of 60bpm corrupted by random amounts of Gaussian noise (standard deviations of 0–500ms in steps of 50ms). Accuracy was assessed by computing the normalized RMSE in the final T_1 and T_2 maps.

Phantom Study

A water and agarose phantom was imaged at 3T (Siemens MAGNETOM Skyra, Erlangen, Germany) to evaluate the accuracy and precision of the proposed MRF sequence compared to conventional parameter mapping. The phantom contained ten vials with values of T_1 200–1530ms and T_2 20–115ms. An artificial ECG signal was simulated at the scanner with a heart rate of 60bpm. The scans were performed using an 18-channel brain receive array and the indwelling body array for excitation. All phantom and in vivo MRF scans used the

following parameters: 300x300mm^2 FoV, 192x192 matrix, spatial resolution 1.6x1.6x8.0mm^3, RF pulse duration 800μs, time bandwidth product 2, TE=0.84ms, and minimum TR=5.10ms. MRF T_1 and T_2 maps were compared with conventional spin echo maps for quantification of T_1 (using TRs from 50–5000ms, scan time 33min) and T_2 (using TEs 15–400ms, scan time 192min). Pixelwise T_1 and T_2 values were calculated by a nonlinear parameter fit to $S(TR)=a+be^{-\frac{TR}{T_1}}$ and $S(TE)=ae^{-\frac{TE}{T_2}}$. Accuracy was assessed by comparing the mean $T_1$and T_2 values from MRF with those from the spin echo experiments, while precision was defined as the standard deviation in T_1 and T_2 over each ROI. Measurements from MRF and spin echo were also compared using linear regression.

Additional phantom data were acquired to evaluate the dependence of MRF on heart rate by using a simulated ECG signal with heart rates ranging from 40–120bpm in steps of 10bpm. The mean T_1 and T_2 values were computed within each ROI at all heart rates.

Human Volunteer Imaging

Eleven asymptomatic volunteers were scanned at 3T in an IRB-approved, HIPAA-compliant study after obtaining written informed consent. Data were acquired with an 18-channel body receive array and a 12-channel spine transmit/receive array. Scans were performed in short-axis orientation at a mid-ventricular level. All volunteers were scanned with MRF and conventional parameter mapping sequences, as described below. The MRF scan lasted 16 heartbeats and was acquired over a single breathhold during expiration, and the trigger delay was adjusted so that the 240–280ms scan window occurred during late diastole; note that this was the same basic acquisition scheme used for simulations and phantom studies. A total of 48 RF excitation pulses was applied every heartbeat to produce 768 images over the entire scan. The timestamp for each RF pulse was used when generating the dictionary in order to account for changes in heart rhythm.

The original 17-heartbeat MOLLI (16) sequence with a 3-(3)-3-(3)-5 sampling scheme and TIs of 120, 200, and 280ms was used to generate gold-standard T_1 maps for comparison with the MRF T_1 maps. A T_2-prepared bSSFP sequence was chosen as the gold-standard for the T_2 comparisons, with a scan time of 9 heartbeats, a 1-(3)-1-(3)-1 sampling scheme, and T_2-preparation times of TE=0, 20, and 50ms. The raw images from the standard T_1 and T_2 mapping sequences were processed using custom software provided by Siemens that performed a non-rigid registration followed by a three-parameter (T_1) or two-parameter (T_2) fit.

All parameter maps were analyzed by drawing ROIs in the left ventricular blood pool and over the entire myocardial wall, and the mean and standard deviation in T_1 and T_2 values were calculated in these areas. A Bland-Altman analysis (37) was performed to evaluate the agreement between MRF and MOLLI and between MRF and the standard T_2 quantification sequence.

Scan Time and Measurement Precision

One volunteer dataset was analyzed to investigate the effect of reduced scan time on map quality. The original MRF dataset consisted of sixteen heartbeats, and maps were generated

using the first four, eight, twelve, and sixteen heartbeats with the iterative denoising pattern recognition. The average and standard deviations in T_1 and T_2 were computed over the entire myocardium for each case.

Results

Simulations

Table 1 presents simulation results that were used to guide the cardiac MRF sequence design, which varied the FA/TR pattern, presence or absence of magnetization preparation pulses, and maximum flip angle. When a constant flip angle and TR were used without magnetization preparation, the errors were lowest for a maximum flip angle of 15° and increased substantially for larger flip angles. As expected, the use of inversions and T_2 preparation produced overall lower RMSE in the reconstructed T_1 and T_2 maps. Over the range of maximum flip angles that were tested, sequences with a variable FA/TR pattern and magnetization preparation pulses produced the smallest errors in the parameter maps. Figure 4 shows the ground truth T_1, T_2, and M_0 maps used in this simulation, as well as MRF reconstructions for the sequences having a maximum flip angle of 15° (corresponding to the leftmost column in Table 1).

Figures 5A and 5B present RMSE values for the second simulation, in which the MRF scan duration was varied between two to sixteen heartbeats. When direct pattern matching was employed, lower errors were obtained for both T_1 and T_2. The T_1 RMSE plateaued around 10% once the scan duration reached eight heartbeats, while the T_2 RMSE continued to decrease to roughly 20% at a scan duration of sixteen heartbeats. The iterative pattern matching produced the most accurate reconstructions in all cases. The lowest errors were obtained when iterative matching was used in combination with a variable FA/TR sequence, with the RMSE reaching a plateau of approximately 7% for T_1 and 9% for T_2 after four heartbeats. With the iterative matching, there was an advantage to using the variable FA/TR pattern when the scan duration was short; however, the RMSE for both variable and constant FA/TR patterns became similar as the scan time increased to sixteen heartbeats. Figure 5C presents results from the variable heart rate simulation. Both T_1 and T_2 quantification were robust to changes in heart rate, even at the most extreme case tested, where noise with a 500ms standard deviation (50% of the average R-R interval) was added to a 60bpm heart rhythm.

Phantom Study

The MRF sequence was validated in a phantom against spin echo as the gold standard. The mean and standard deviations in T_1 and T_2 from both methods in each region of the phantom are shown in Figure 6A using a constant simulated heart rate of 60bpm. Both MRF and spin echo measurements are in good agreement and display a strong linear trend (R^2=0.998 for T_1, and R^2=0.991 for T_2). The best fit lines had slopes of 1.06 (T_1) and 1.03 (T_2), and y-intercepts of −0.58ms (T_1) and 0.95ms (T_2). In addition, consistent T_1 and T_2 measurements were obtained over a range of simulated heart rates between 40–120bpm (Figure 6B). The errors bars indicate the standard deviations within each homogeneous region of the phantom.

Human Volunteer Imaging

T_1, T_2, and M_0 maps were successfully acquired in eleven asymptomatic volunteers at 3T using MRF, MOLLI, and a bSSFP sequence with multiple T_2 preparation times. ROIs were drawn over the entire myocardial wall, and the mean and standard deviation in T_1, T_2, and M_0 for all volunteers are listed in Sup Table S1. Over all volunteers, the mean T_1 measured in the myocardium with MRF was 1235ms (min 1199ms, max 1316ms), which agrees well with the mean T_1 measured with MOLLI of 1247ms (min 1206ms, max 1297ms). For T_2, the mean myocardial value measured with MRF was 38ms (min 34ms, max 43ms), which is consistent with the mean value obtained with the T_2-prepared bSSFP sequence of 38ms (min 32ms, max 43ms). These measurements lie within the range of previously reported native myocardial relaxation times at 3T of T_1 from 1080–1500ms (16,18,24,38) and T_2 from 38–50ms (24,39). The mean M_0 measured in myocardium was 0.28 but exhibited wide variability across subjects (min 0.12, max 0.39). Measurements of T_1, T_2, and M_0 in the blood pool may not be reliable since spins entering and leaving the imaging plane cannot be simulated accurately. Nevertheless, in the LV blood pool, the mean T_1 measured with MRF over all volunteers was 1807ms (min 1701ms, max 1931ms) and the mean T_2 was 91ms (min 76ms, max 107ms). The blood T_1 measurements are in agreement with literature values of 1550–1932ms (40–43); however, the blood T_2 measurements obtained with both MRF and T_2-prepared bSSFP are lower than in previously reported studies, which found T_2 values in oxygenated blood of 175ms (44) to 275ms (40).

Representative maps from one volunteer are shown in Figure 7. Visually, the MRF maps have few obvious artifacts, and the myocardial wall appears homogeneous. In the left ventricular wall, MRF produced values of T_1=1213±75ms and T_2=34.9±3.8ms, while MOLLI and T_2-prepared bSSFP yielded T_1=1257±61ms and T_2=41.6±5.0ms. In the LV blood pool, MRF produced measurements of T_1=1838±39ms and T_2=112±7ms, while the conventional methods yielded T_1=1855±43ms and T_2=100±11ms. One interesting feature visible on maps from all sequences is the elevated T_2 in the left ventricular blood pool compared to the right (125±5ms compared to 86±10ms, respectively, for this volunteer).

A Bland-Altman analysis was performed to assess the agreement between MRF and the conventional mapping sequences (Figure 8). In the myocardium, T_1 measurements acquired with MOLLI and MRF from all volunteers were within the 95% limits of agreement (−78ms to 79ms). The mean bias was 1ms, and the maximum and minimum differences were 72ms and −72ms, respectively. Similarly, all T_2 measurements acquired with MRF and T_2-prepared bSSFP were within the 95% limits of agreement (−8.5ms to 3.3ms). The mean bias was −2.6ms, and the maximum and minimum differences were 3.1ms and −6.7ms, respectively. The same analysis was applied to the measurements averaged over the left ventricular blood pool. For T_1, the 95% limits of agreement were −87ms to 91ms with a mean bias of 2ms, and one volunteer data point was outside the limits of agreement (−107ms lower T_1 with MRF than MOLLI). For T_2, the 95% limits of agreement were −3.4 to 21.9ms with a mean bias of 9.2ms, and one measurement was outside the limits of agreement (−3.8ms lower T_2 with MRF than the conventional sequence).

Scan Time and Measurement Precision

Figure 9 shows MRF T_1 and T_2 maps from a single volunteer reconstructed using the first four, eight, twelve, and sixteen heartbeats of the original dataset. Visually, the maps appear similar but with increased noise at the shorter scan times, which is corroborated by the higher standard deviations in T_1 and T_2 measured over the myocardial wall (Figure 9, bottom). The average estimated T_1 increased slightly for shorter scan times (1230ms for 16 heartbeats compared to 1275ms for 4 heartbeats). Conversely, the estimated T_2 decreased somewhat for shorter scan times (36.1ms for 16 heartbeats compared to 33.3ms for 4 heartbeats).

Discussion

This study presents the first application of MR Fingerprinting for quantification of T_1, T_2, and proton spin density in the myocardium using an ECG triggered, breathheld scan. Unlike conventional parameter mapping, in which several T_1 or T_2 weighted images are acquired while signals are in steady state, MRF uses a flexible schedule of flip angles, TRs, and preparation pulses to generate unique timecourses for each discrete combination of T_1 and T_2. The MRF T_1 measurements in healthy volunteers displayed good agreement with MOLLI, as shown in the Bland-Altman analysis (Figure 8). There are two data points that lie within the 95% limits of agreement but still show a large (roughly 80ms) discrepancy between MRF and MOLLI, which may be due to residual cardiac motion during the scan window. Although it has been reported that MOLLI consistently underestimates T_1 for long T_1 values and fast heart rates (17), the measurements obtained with MOLLI in this study were longer and more consistent with those reported in (45). Additionally, the T_2 measurements between MRF and the conventional sequence agreed well with a mean bias −2.6ms in the Bland-Altman analysis. Ongoing work will address the wide variability observed in the in vivo proton density maps, potentially caused by coil shading, flow-induced artifacts, or other sources of error not explored in this study.

MRF demonstrated a high degree of independence from heart rate in the simulation and phantom studies. This property arises because the time that elapses between the end of one acquisition window and the first RF excitation in the next heartbeat, which changes according to the subject's heart rhythm, is logged at the scanner and then incorporated in the Bloch simulation. This is in contrast to traditional parameter mapping, where changes in heart rate are typically viewed as detrimental. Additionally, this paradigm is different from other MRF applications where it is possible to define all aspects of the pulse sequence a priori, and then precompute a single dictionary that can be applied to subsequent scans. With cardiac MRF, a new dictionary is generated after every scan.

The MRF pulse sequence implemented here uses a limited range of flip angles and TRs for practical reasons. Much of the T_1 and T_2 contrast in the current implementation is generated by the different magnetization preparation pulses, with a smaller contribution coming from the variable flip angle and TR pattern. Thus, discrepancies in the actual flip angles due to an imperfect slice profile or inhomogeneous B_1^+ do not appreciably change the measured T_1 and T_2 values, similar to the findings in (24). Also, adiabatic inversion and T_2 preparation pulses were chosen for their robustness to B_0 and B_1^+ inhomogeneities at 3T. Simulation

results (Table 1) showed nearly equivalent accuracy in the T_1 and T_2 estimation when the maximum flip angle was varied between 15 to 75 degrees, provided that the sequence employed a variable FA/TR schedule and included inversions and T_2 preparation. Thus, allowing a larger flip angle variation may not substantially improve the diversity in the MRF dictionary, although the increased signal level could reduce noise in the final parameter maps. However, moving to larger flip angles at 3T may require both modeling the actual slice profile, and either including B_1 as an additional parameter in the dictionary (46,47) or acquiring a separate B_1 field map (48). Similarly, the TRs were varied over a relatively narrow range of 5.1–6.1ms. This ensured that the TRs were short, which increased the number of images that could be acquired every heartbeat to aid in pattern matching. Techniques to shorten RF pulse duration, such as the use of VERSE (49) rather than sinc pulses, could allow a wider range of TR variations without reducing the number of images that can be collected inside the limited scan window. Once these technical hurdles are overcome, the cardiac MRF framework could be generalized to more exotic pulse sequences, such as those with larger flip angles and less reliance on preparation modules.

Several interesting features regarding the MRF pulse sequence design are apparent from Table 1. Excellent accuracy in the T_1 and T_2 estimates was obtained when using a variable FA/TR series with inversions and T_2 preparation over a range of maximum flip angles. However, when using a constant FA/TR, the errors in T_1 and T_2 increased substantially as the maximum flip angle increased beyond 25°. We speculate that sequences which produce smoothly varying signal timecourses are incoherent with respect to the aliasing artifacts from the spiral undersampling, which corrupt the measured timecourses with high frequency noise. Thus, when using a constant FA/TR schedule, large flip angles produce timecourses with high frequency oscillations that are difficult to separate from the aliasing artifacts, while small flip angles produce more smoothly varying timecourses. Similarly, the variable FA/TR schedule uses gradual changes in flip angles to avoid high frequency oscillations.

It is important to note that significant motion during the MRF data acquisition may lead to inaccurate parameter values. Flow will cause spins entering or leaving the slice plane to experience a magnetization history that differs from the dictionary simulation. Thus, the blood T_1, T_2, and M_0 obtained with MRF may not be reliable. In addition, the relatively long 250ms scan window may need to be shortened in order to scan patients with rapid heart rates. Residual in-plane motion could lead to blurring or partial volume artifacts, while through-plane motion will cause spins to move outside the imaging plane.

Rapid computation time is important when introducing new methods to the clinic. In this study, generating the dictionary only took 12s on a desktop PC. The main bottleneck was due to the iterative pattern recognition, which required almost 8 minutes per slice. This processing time could be reduced by using optimized code or parallel computing. Alternatively, direct pattern matching could be used, which only required 33s per slice. Direct pattern matching produced maps with similar quality as the iterative denoising algorithm when longer scan times (e.g. 16 heartbeats) were permitted, as seen in Figure 5; however, at shorter scan times, the iterative reconstruction was superior. Therefore, direct pattern matching could be used for faster online reconstructions if a sufficient number of MRF images is available.

Cardiac MRF is one of several techniques that can perform simultaneous T_1 and T_2 mapping in the myocardium, including CAIBIRIA (23), QALAS (24), and joint T_1-T_2 mapping with T_2-preparation and either saturation (25) or inversion pulses (26). Although the use of interleaved inversions and T_2 preparations is used in other mapping sequences, the MRF paradigm is unique in several ways. Highly undersampled images are acquired on a rapid time scale every TR, in contrast to single-shot techniques that collect entire images over a longer temporal footprint. This introduces additional flexibility in the MRF sequence design since signal timecourses are not restricted to be near steady state, as with single-shot techniques. Quantitative MRF maps are generated using pattern matching, which is inherently robust to signal deviations from sources such as noise, aliasing, or motion that are not present in the dictionary. Thus, MRF does not require explicit registration of the raw images before generating the parametric maps. Additionally, many techniques that use nonlinear parameter fitting require relaxation heartbeats to allow the longitudinal magnetization to recover, which decreases scan efficiency. MRF does not have this limitation due to its use of a Bloch simulation and pattern matching.

One limitation of this first cardiac MRF implementation is the relatively long breathhold duration (16 heartbeats) and acquisition window (240–280ms), which may not be feasible for patients who have difficulty holding their breath or have very rapid heart rates or arrhythmias. It was demonstrated that MRF scans could be performed in as short as 4–8 heartbeats at the expense of increased noise in the final maps. In general, scanning for a longer time may reduce the quantification errors by providing new information that will aid the pattern matching. Future work will investigate ways to reduce the total number of images required (and thus shorten the breathhold duration), as well as decrease the number of RF excitations per heartbeat to reduce blurring from myocardial wall motion. Pulse sequence optimization can be used to find a pattern of flip angles, TRs, and preparation pulses that will create a dictionary with orthogonal signal evolutions and high SNR. Scan time could be further reduced by combining MRF with parallel imaging or compressed sensing reconstructions. Finally, the MRF framework is flexible and could potentially map additional parameters within the same scan, such as T_2* or $T_{1\rho}$.

Conclusion

The proposed ECG-triggered cardiac MRF sequence enables robust and reproducible measurements of T_1, T_2, and M_0 in the myocardial wall within a single breathhold of sixteen heartbeats or less. Phantom studies showed that MRF produced measurements that agree with conventional spin echo and are robust over a range of heart rates. The MRF scan was tested in healthy volunteers and was consistent with T_1 measurements from MOLLI and T_2 measurements from T_2-prepared bSSFP. MRF is a promising new candidate for rapid and accurate cardiac parameter mapping but requires additional validation in patients.

Supplementary Material

Refer to Web version on PubMed Central for supplementary material.

Acknowledgments

This work was funded by the NIH (T32EB007509 and 2KL2TR000440), NIH/NIBIB (R00EB011527) and Siemens Medical Solutions (Erlangen, Germany).

References

1. Sibley CT, Noureldin RA, Gai N, et al. T1 Mapping in Cardiomyopathy at Cardiac MR: Comparison with Endomyocardial Biopsy. Radiology. 2012; 265:724–732. [PubMed: 23091172]
2. Roller FC, Harth S, Schneider C, Krombach GA. T1, T2 Mapping and Extracellular Volume Fraction (ECV): Application, Value and Further Perspectives in Myocardial Inflammation and Cardiomyopathies. Rofo. 2015; 187:760–770. [PubMed: 26098250]
3. Hinojar R, Nagel E, Puntmann VO. T1 mapping in myocarditis - headway to a new era for cardiovascular magnetic resonance. Expert Rev Cardiovasc Ther. 2015; 13:871–874. [PubMed: 26018769]
4. Goldfarb JW, Arnold S, Han J. Recent myocardial infarction: assessment with unenhanced T1-weighted MR imaging. Radiology. 2007; 245:245–250. [PubMed: 17885192]
5. Okur A, Kantarcı M, Kızrak Y, Yıldız S, Pirimoğlu B, Karaca L, Oğul H, Sevimli S. Quantitative evaluation of ischemic myocardial scar tissue by unenhanced T1 mapping using 3.0 Tesla MR scanner. Diagn Interv Radiol. 20:407–413. [PubMed: 25010366]
6. Dall'Armellina E, Piechnik SK, Ferreira VM, et al. Cardiovascular magnetic resonance by non contrast T1-mapping allows assessment of severity of injury in acute myocardial infarction. J Cardiovasc Magn Reson. 2012; 14:15. [PubMed: 22309452]
7. Bull S, White SK, Piechnik SK, et al. Human non-contrast T1 values and correlation with histology in diffuse fibrosis. Heart. 2013; 99:932–937. [PubMed: 23349348]
8. Karamitsos TD, Piechnik SK, Banypersad SM, et al. Noncontrast T1 mapping for the diagnosis of cardiac amyloidosis. JACC Cardiovasc Imaging. 2013; 6:488–497. [PubMed: 23498672]
9. Moon JC, Messroghli DR, Kellman P, et al. Myocardial T1 mapping and extracellular volume quantification: a Society for Cardiovascular Magnetic Resonance (SCMR) and CMR Working Group of the European Society of Cardiology consensus statement. J Cardiovasc Magn Reson. 2013; 15:92. [PubMed: 24124732]
10. Kellman P, Wilson JR, Xue H, Bandettini WP, Shanbhag SM, Druey KM, Ugander M, Arai AE. Extracellular volume fraction mapping in the myocardium, part 2: initial clinical experience. J Cardiovasc Magn Reson. 2012; 14:64. [PubMed: 22967246]
11. Ugander M, Oki A, Hsu L. Extracellular volume imaging by magnetic resonance imaging provides insights into overt and sub-clinical myocardial pathology. Eur Heart J. 2012; 33:1268–1278. [PubMed: 22279111]
12. Park CH, Choi E-Y, Kwon HM, et al. Quantitative T2 mapping for detecting myocardial edema after reperfusion of myocardial infarction: validation and comparison with T2-weighted images. Int J Cardiovasc Imaging. 2013; 29(Suppl 1):65–72. [PubMed: 23765068]
13. Giri S, Chung Y-C, Merchant A, Mihai G, Rajagopalan S, Raman SV, Simonetti OP. T2 quantification for improved detection of myocardial edema. J Cardiovasc Magn Reson. 2009; 11:56. [PubMed: 20042111]
14. Butler CR, Savu A, Bakal JA, et al. Correlation of cardiovascular magnetic resonance imaging findings and endomyocardial biopsy results in patients undergoing screening for heart transplant rejection. J Heart Lung Transplant. 2015; 34:643–650. [PubMed: 25934478]
15. Thavendiranathan P, Walls M, Giri S, Verhaert D, Rajagopalan S, Moore S, Simonetti OP, Raman SV. Improved detection of myocardial involvement in acute inflammatory cardiomyopathies using T2 mapping. Circ Cardiovasc Imaging. 2012; 5:102–110. [PubMed: 22038988]
16. Messroghli DR, Radjenovic A, Kozerke S, Higgins DM, Sivananthan MU, Ridgway JP. Modified Look-Locker inversion recovery (MOLLI) for high-resolution T1 mapping of the heart. Magn Reson Med. 2004; 52:141–146. [PubMed: 15236377]
17. Piechnik SK, Ferreira VM, Dall'Armellina E, Cochlin LE, Greiser A, Neubauer S, Robson MD. Shortened Modified Look-Locker Inversion recovery (ShMOLLI) for clinical myocardial T1-

mapping at 1. 5 and 3 T within a 9 heartbeat breathhold. J Cardiovasc Magn Reson. 2010; 12:69. [PubMed: 21092095]

18. Chow K, Flewitt JA, Green JD, Pagano JJ, Friedrich MG, Thompson RB. Saturation recovery single-shot acquisition (SASHA) for myocardial T1 mapping. Magn Reson Med. 2014; 71:2082–2095. [PubMed: 23881866]
19. Marie PY, Angioï M, Carteaux JP, et al. Detection and prediction of acute heart transplant rejection with the myocardial T2 determination provided by a black-blood magnetic resonance imaging sequence. J Am Coll Cardiol. 2001; 37:825–831. [PubMed: 11693758]
20. De Roquefeuil M, Vuissoz P-A, Escanyé J-M, Felblinger J. Effect of physiological heart rate variability on quantitative T2 measurement with ECG-gated Fast Spin Echo (FSE) sequence and its retrospective correction. Magn Reson Imaging. 2013; 31:1559–1566. [PubMed: 23954080]
21. Sprinkart AM, Luetkens JA, Träber F, et al. Gradient Spin Echo (GraSE) imaging for fast myocardial T2 mapping. J Cardiovasc Magn Reson. 2015; 17:12. [PubMed: 25885268]
22. Huang TY, Liu YJ, Stemmer A, Poncelet BP. T2 measurement of the human myocardium using a T 2-prepared transient-state trueFISP sequence. Magn Reson Med. 2007; 57:960–966. [PubMed: 17457877]
23. Santini F, Kawel-Boehm N, Greiser A, Bremerich J, Bieri O. Simultaneous T1 and T2 quantification of the myocardium using cardiac balanced-SSFP inversion recovery with interleaved sampling acquisition (CABIRIA). Magn Reson Med. 2014; 74:365–371. [PubMed: 25113911]
24. Kvernby S, Warntjes MJB, Haraldsson H, Carlhäll C-J, Engvall J, Ebbers T. Simultaneous three-dimensional myocardial T1 and T2 mapping in one breath hold with 3D-QALAS. J Cardiovasc Magn Reson. 2014; 16:102. [PubMed: 25526880]
25. Akçakaya M, Weingärtner S, Basha TA, Roujol S, Bellm S, Nezafat R. Joint myocardial T1 and T2 mapping using a combination of saturation recovery and T2 -preparation. Magn Reson Med. 2015; doi: 10.1002/mrm.25975
26. Blume U, Lockie T, Stehning C, Sinclair S, Uribe S, Razavi R, Schaeffter T. Interleaved T1 and T2 relaxation time mapping for cardiac applications. J Magn Reson Imaging. 2009; 29:480–487. [PubMed: 19161206]
27. Weingärtner S, Roujol S, Akçakaya M, Basha TA, Nezafat R. Free-breathing multislice native myocardial T1 mapping using the slice-interleaved T1 (STONE) sequence. Magn Reson Med. 2014; 74:115–124.
28. Ma D, Gulani V, Seiberlich N, Liu K, Sunshine JL, Duerk JL, Griswold Ma. Magnetic resonance fingerprinting. Nature. 2013; 495:187–92. [PubMed: 23486058]
29. Jiang Y, Ma D, Seiberlich N, Gulani V, Griswold MA. MR fingerprinting using fast imaging with steady state precession (FISP) with spiral readout. Magn Reson Med. 2015; 74:1621–1631. [PubMed: 25491018]
30. Perlin K. An image synthesizer. ACM SIGGRAPH Comput Graph. 1985; 19:287–296.
31. Brittain JH, Hu BS, Wright GA, Meyer CH, Macovski A, Nishimura DG. Coronary angiography with magnetization-prepared T2 contrast. Magn Reson Med. 1995; 33:689–696. [PubMed: 7596274]
32. Hargreaves, BA. [Accessed June 1, 2014] Variable-Density Spiral Design Functions. Updated September 9, 2005http://www-mrsrl.stanford.edu/~brian/vdspiral/
33. Fessler JA. On NUFFT-based gridding for non-Cartesian MRI. J Magn Reson. 2007; 188:191–195. [PubMed: 17689121]
34. Pierre EY, Ma D, Chen Y, Badve C, Griswold MA. Multiscale reconstruction for MR fingerprinting. Magn Reson Med. 2015; doi: 10.1002/mrm.25776
35. Walsh D, Gmitro A, Marcellin M. Adaptive reconstruction of phased array MR imagery. Magn Reson Med. 2000; 43:682–90. [PubMed: 10800033]
36. Wissmann L, Santelli C, Segars WP, Kozerke S. MRXCAT: Realistic numerical phantoms for cardiovascular magnetic resonance. J Cardiovasc Magn Reson. 2014; 16:63. [PubMed: 25204441]
37. Bland JM, Altman DG. Statistical methods for assessing agreement between two methods of clinical measurement. Lancet. 1986; 1:307–310. [PubMed: 2868172]

38. Fitts M, Breton E, Kholmovski EG, Dosdall DJ, Vijayakumar S, Hong KP, Ranjan R, Marrouche NF, Axel L, Kim D. Arrhythmia insensitive rapid cardiac T1 mapping pulse sequence. Magn Reson Med. 2013; 70:1274–82. [PubMed: 23280998]
39. Van Heeswijk RB, Feliciano H, Bongard C, Bonanno G, Coppo S, Lauriers N, Locca D, Schwitter J, Stuber M. Free-breathing 3 T magnetic resonance T2-mapping of the heart. JACC Cardiovasc Imaging. 2012; 5:1231–1239. [PubMed: 23236973]
40. Stanisz GJ, Odrobina EE, Pun J, Escaravage M, Graham SJ, Bronskill MJ, Henkelman RM. T1, T2 relaxation and magnetization transfer in tissue at 3T. Magn Reson Med. 2005; 54:507–512. [PubMed: 16086319]
41. Greenman RL, Shirosky JE, Mulkern RV, Rofsky NM. Double inversion black-blood fast spin-echo imaging of the human heart: a comparison between 1.5T and 3. 0T. J Magn Reson Imaging. 2003; 17:648–55. [PubMed: 12766893]
42. Lu H, Clingman C, Golay X, van Zijl PCM. Determining the longitudinal relaxation time (T1) of blood at 3. 0 Tesla. Magn Reson Med. 2004; 52:679–82. [PubMed: 15334591]
43. Shimada K, Nagasaka T, Shidahara M, Machida Y, Tamura H. In vivo measurement of longitudinal relaxation time of human blood by inversion-recovery fast gradient-echo MR imaging at 3T. Magn Reson Med Sci. 2012; 11:265–71. [PubMed: 23269013]
44. Chen JJ, Pike GB. Human whole blood T2 relaxometry at 3 Tesla. Magn Reson Med. 2009; 61:249–54. [PubMed: 19165880]
45. Nacif MS, Turkbey EB, Gai N, et al. Myocardial T1 mapping with MRI: Comparison of look-locker and MOLLI sequences. J Magn Reson Imaging. 2011; 34:1367–1373. [PubMed: 21954119]
46. Cloos, M., Zhao, T., Knoll, F., Alon, L., Lattanzi, R., Sodickson, DK. Magnetic Resonance Fingerprint Compression. Proceedings of the 23rd Annual Meeting of ISMRM; Toronto, Canada. 2015. p. 330
47. Buonincontri G, Sawiak SJ. MR fingerprinting with simultaneous B1 estimation. Magn Reson Med. 2015; doi: 10.1002/mrm.26009
48. Chen, Y., Jiang, Y., Ma, D., Wright, KL., Seiberlich, N., Griswold, MA., Gulani, V. Magnetic resonance fingerprinting (MRF) for rapid quantitative abdominal imaging. Proceedings of the 22nd Annual Joint Annual Meeting of ISMRM-ESMRMB; Milan, Italy. 2014. p. 561
49. Hargreaves BA, Cunningham CH, Nishimura DG, Conolly SM. Variable-rate selective excitation for rapid MRI sequences. Magn Reson Med. 2004; 52:590–597. [PubMed: 15334579]

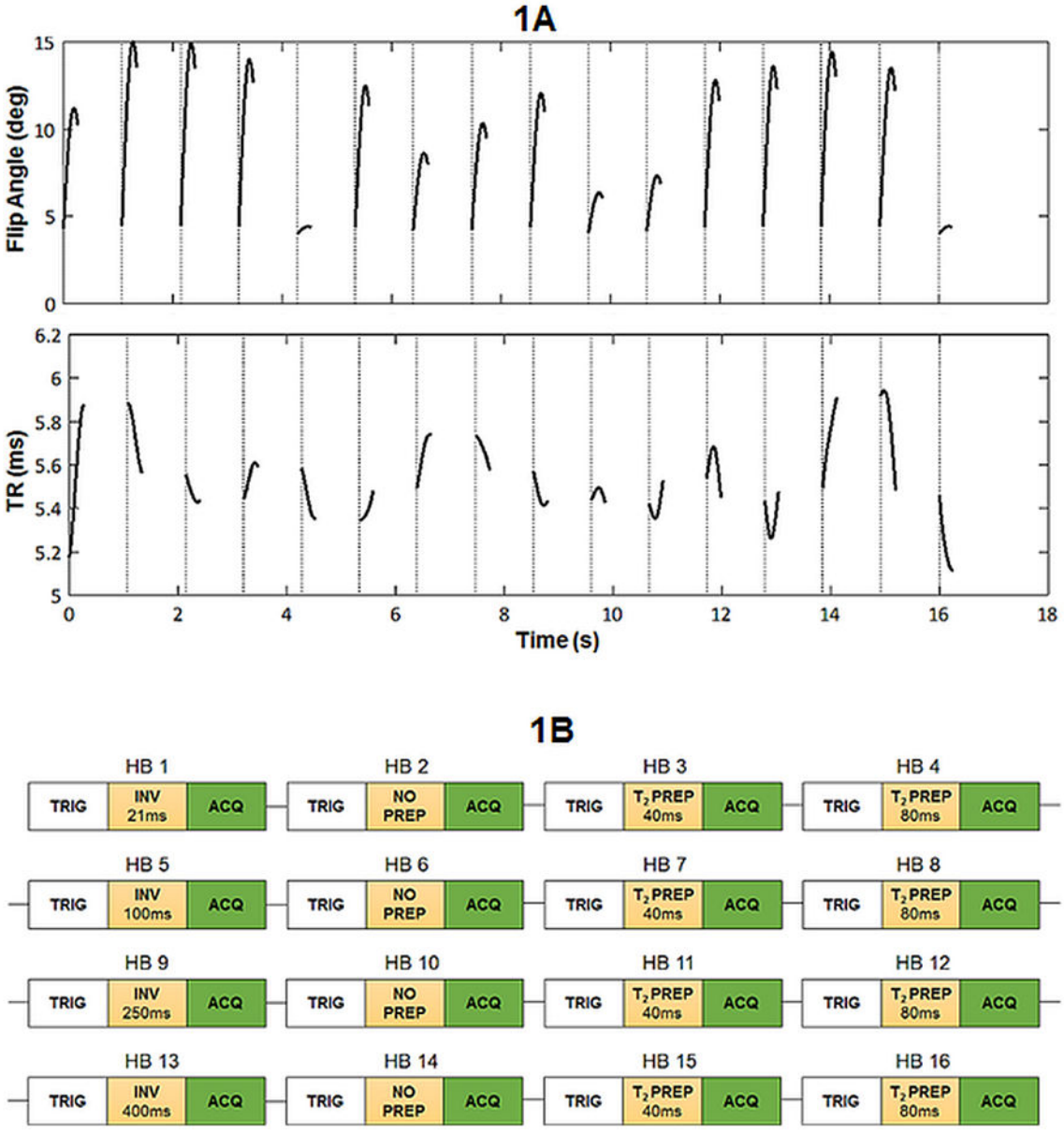

Figure 1.

(a) Diagram of the cardiac MRF pulse sequence with time-varying flip angles (4–15°) and TRs (5.1–6.1ms). **(b)** Each heartbeat consists of a fixed trigger delay, a magnetization preparation pulse (either inversion, T_2 preparation, or no preparation), and a data acquisition window with a fixed number of spiral interleaves.

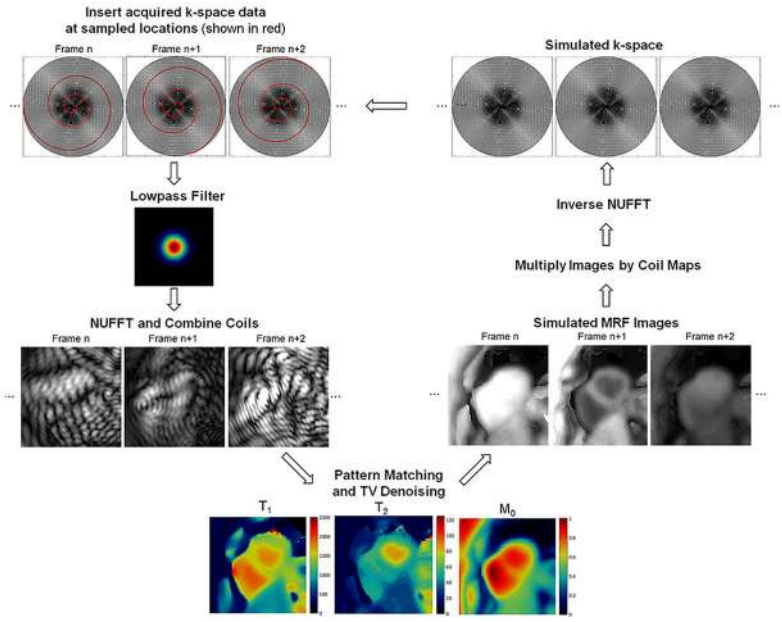

Figure 2.

Steps in the iterative multiscale pattern recognition method. The multi-channel k-space data are lowpass filtered with a Gaussian function every iteration and gridded. The coil images are combined to yield a series of highly undersampled (R=48) images with reduced spatial resolution. The complex-valued signal timecourses are matched to a dictionary to give the intermediate T_1, T_2, and M_0 maps, which then undergo an optional total variation denoising step. Next, MRF signal evolutions are simulated using the intermediate maps. They are multiplied by the coil sensitivity maps and inverse gridded to spiral k-space. Then the acquired k-space data are reinserted at the sampled locations with less aggressive Gaussian filtering on subsequent iterations. The final iteration is performed without lowpass filtering or TV denoising.

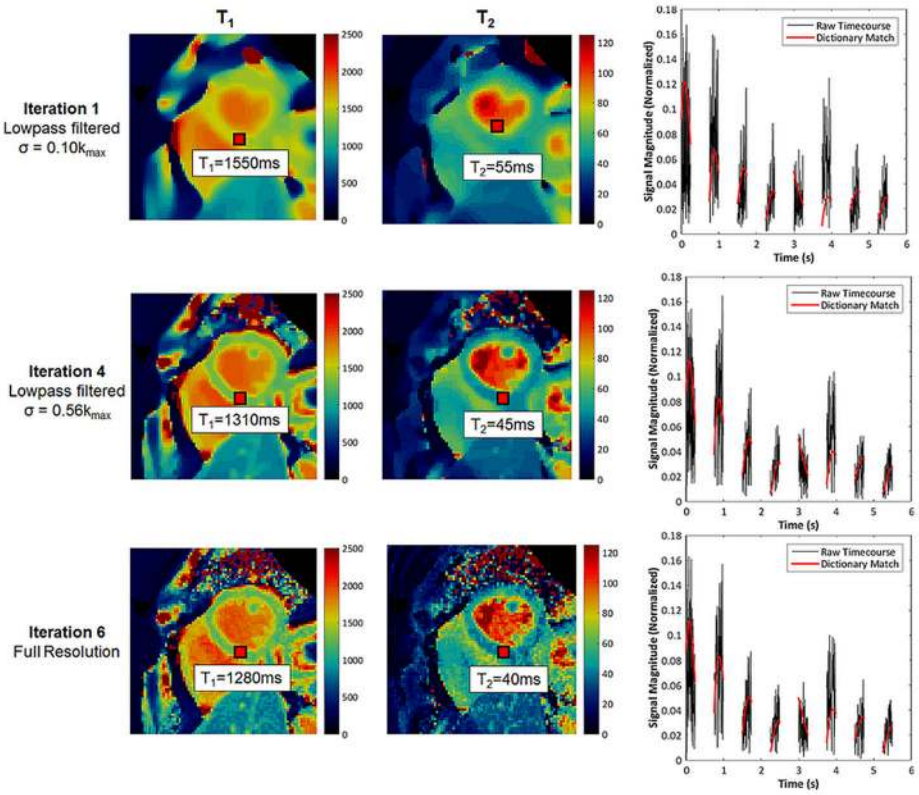

Figure 3.

Parameter maps and example signal timecourses for one volunteer dataset after different iterations of the pattern recognition algorithm. Signal evolutions from one pixel in the myocardium (indicated by the red square) are plotted in black with the closest dictionary match plotted in red. Results are shown after the first, fourth, and final (sixth) iteration.

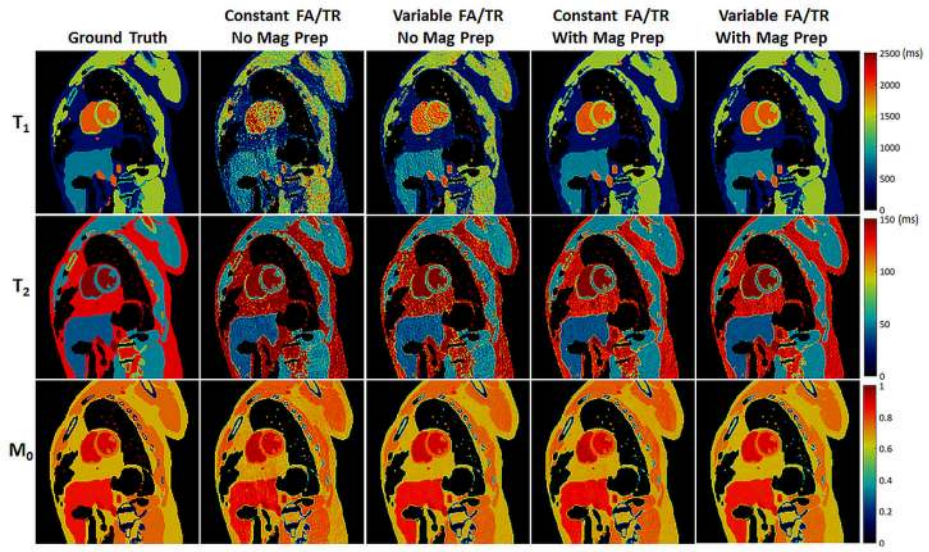

Figure 4.

Simulation results showing ground truth maps and MRF reconstructions for four pulse sequences (variable vs constant FA/TR, and with vs without magnetization preparation). Note that these cases correspond to the leftmost column in Table 1 (where the maximum flip angle is 15°).

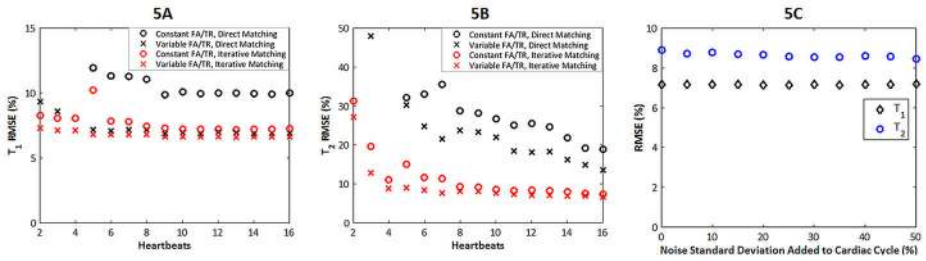

Figure 5.

Simulation results comparing **(a)** T_1 and **(b)** T_2 accuracy in a cardiac phantom using pulse sequences with constant and time-varying flip angle (FA) and TR patterns. Maps were generated both by direct pattern matching and iterative multiscale pattern recognition. **(c)** Plot of the T_1 and T_2 accuracy for 4-heartbeat MRF in the presence of variable heart rates, which were produced by adding Gaussian noise to a 60bpm cardiac rhythm.

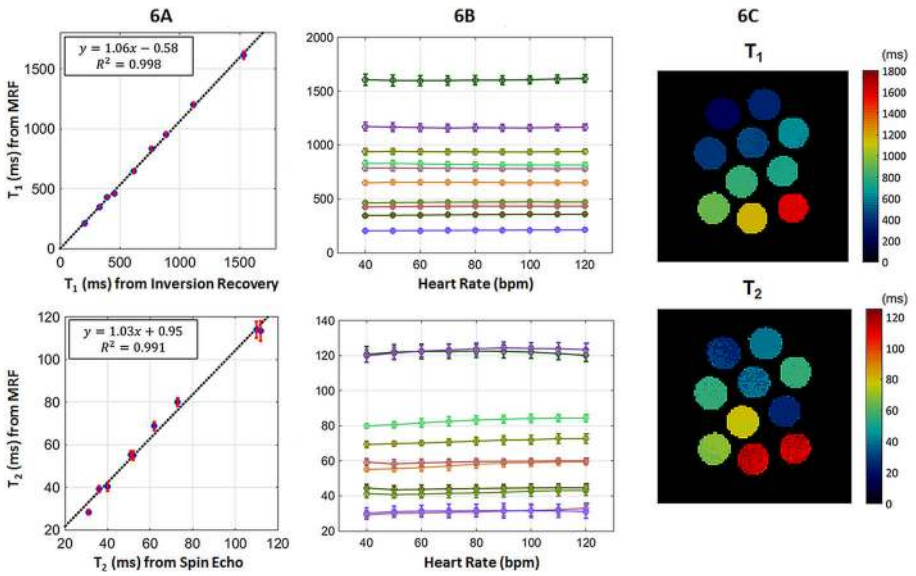

Figure 6.

(a) Phantom results comparing MRF measurements with conventional spin echo. The error bars show the standard deviation over all pixels in each region of the phantom. **(b)** Similar results showing the precision of MRF over a range of simulated heart rates. **(c)** T_1 and T_2 maps acquired with MRF at a simulated 60bpm heart rate showing the phantom structure.

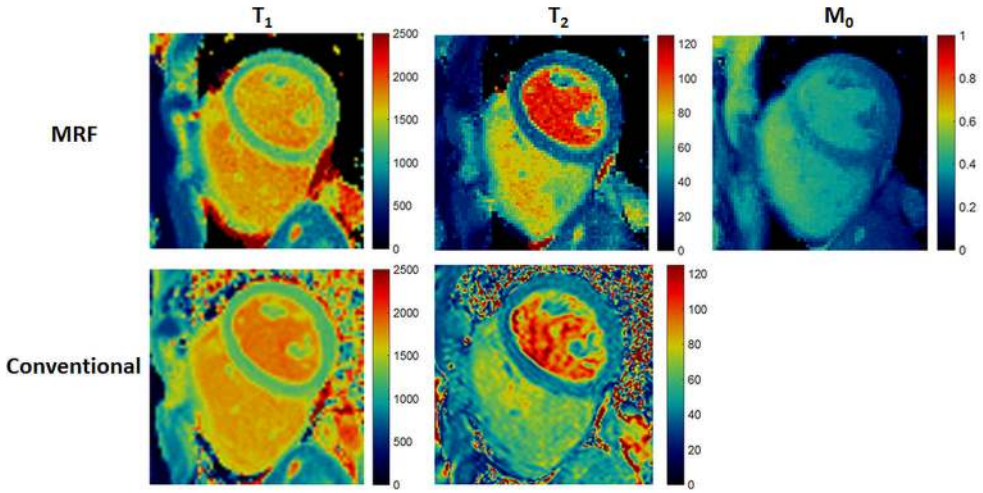

Figure 7.

Maps from one volunteer of T_1, T_2, and M_0 acquired with MRF (top row), MOLLI (bottom left), and a balanced SSFP sequence with three T_2 preparation times (bottom middle).

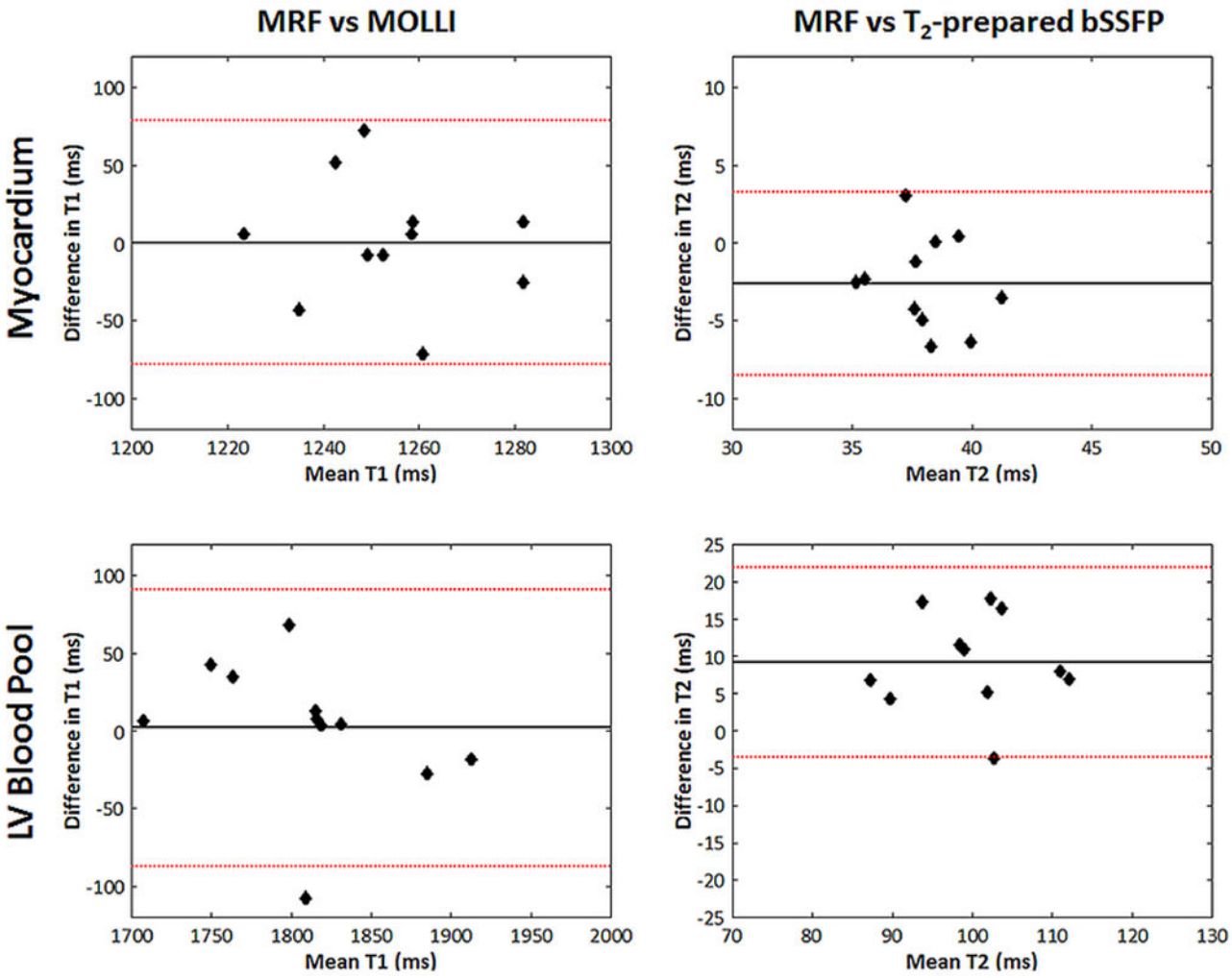

Figure 8.

Bland-Altman plots comparing T_1 between MOLLI and MRF and T_2 between MRF and bSSFP with multiple T_2 preparation times in the myocardium (top row) and left ventricular blood pool (bottom row). The 95% limits of agreement are indicated by dotted red lines, and the mean bias is indicated by the solid black line.

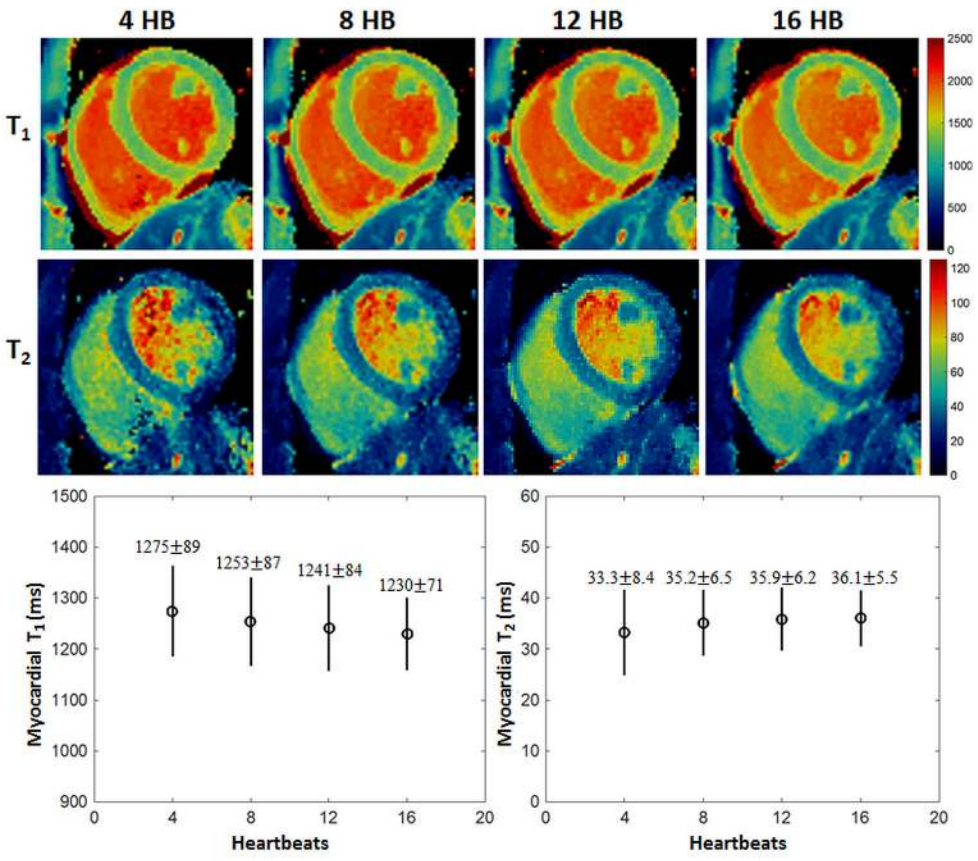

Figure 9.

MRF data were acquired over 16 heartbeats, and maps of T_1, T_2, and M_0 were reconstructed using images from the first four, eight, twelve and sixteen heartbeats. The mean and standard deviation in T_1 and T_2 over the myocardial wall for each case are displayed on the right.

Table 1

MRF T_1 and T_2 Accuracy (Normalized RMSE %)

Accuracy, as measured using normalized RMSE (%), in T_1 and T_2 using a simulated cardiac phantom with different MRF pulse sequence designs. The results are presented such that 8.0/11.3, for example, indicates a normalized RMSE of 8.0% for T_1 and 11.3% for T_2. Twenty-eight sequences were generated by adjusting the following design parameters: (1) variable vs constant FA/TR series, (2) presence or absence of magnetization preparation (inversions and T_2 preparation), and (3) maximum flip angle. The sequence used for the subsequent phantom and in vivo scans is highlighted in yellow.

FA/TR Series	Mag. Prep.	Maximum Flip Angle						
		15°	25°	35°	45°	55°	65°	75°
Constant	With	8.0/11.3	9.2/13.4	21.3/32.0	252.0/76.3	407.2/87.3	465.5/93.1	455.0/93.2
Variable	With	7.1/9.0	7.3/10.1	7.3/8.3	7.3/8.5	7.3/8.8	7.4/9.0	7.3/8.8
Constant	Without	33.5/22.5	31.8/28.1	52.4/39.8	265.2/76.5	454.4/90.1	483.9/92.9	485.1/93.1
Variable	Without	18.9/18.8	19.2/26.3	20.7/18.4	20.5/19.0	18.6/17.6	16.4/15.5	16.1/15.5